BRAIN
REVIEW ARTICLE

Neuromelanin-sensitive MRI as a promising biomarker of catecholamine function

Paula Trujillo, Megan A. Aumann and Daniel O. Claassen

Disruptions to dopamine and noradrenergic neurotransmission are noted in several neurodegenerative and psychiatric disorders. Neuromelanin-sensitive (NM)-MRI offers a non-invasive approach to visualize and quantify the structural and functional integrity of the substantia nigra and locus coeruleus. This method may aid in the diagnosis and quantification of longitudinal changes of disease and could provide a stratification tool for predicting treatment success of pharmacological interventions targeting the dopaminergic and noradrenergic systems. Given the growing clinical interest in NM-MRI, understanding the contrast mechanisms that generate this signal is crucial for appropriate interpretation of NM-MRI outcomes and for the continued development of quantitative MRI biomarkers that assess disease severity and progression. To date, most studies associate NM-MRI measurements to the content of the neuromelanin pigment and/or density of neuromelanin-containing neurons, while recent studies suggest that the main source of the NM-MRI contrast is not the presence of neuromelanin but the high-water content in the dopaminergic and noradrenergic neurons. In this review, we consider the biological and physical basis for the NM-MRI contrast and discuss a wide range of interpretations of NM-MRI. We describe different acquisition and image processing approaches and discuss how these methods could be improved and standardized to facilitate large-scale multisite studies and translation into clinical use. We review the potential clinical applications in neurological and psychiatric disorders and the promise of NM-MRI as a biomarker of disease, and finally, we discuss the current limitations of NM-MRI that need to be addressed before this technique can be utilized as a biomarker and translated into clinical practice and offer suggestions for future research.

Department of Neurology, Vanderbilt University Medical Center, Nashville, TN 37212, USA

Correspondence to: Paula Trujillo, PhD
Department of Neurology, Vanderbilt University Medical Center
1161 21st Ave South A-0118
Nashville, TN 37212, USA
E-mail: paula.trujillo@vumc.org

Keywords: neuromelanin; MRI; dopamine; noradrenaline; catecholamine

Introduction

Advances in neuroimaging have afforded new opportunities to detect structural and functional disruptions to catecholamine networks, which play a critical role in the progression of several neurodegenerative and psychiatric disorders. It is imperative to employ advanced techniques to study diseases such as Parkinson's disease, Alzheimer's disease, schizophrenia and depression, for which there is no curative therapy. While various monoamine-based therapeutic strategies are used in clinical practice, it is crucial to develop biomarkers that advance our understanding of the pathophysiology of neurodegenerative and psychiatric diseases, refining differential diagnosis, identifying symptomatic and prodromal stages, offering insights to prognosis and disease progression, and demonstrating target validation of experimental therapeutics. Dopamine and noradrenaline play significant roles in controlling brain states, vigilance, action, reward, learning and memory processes; therefore, biomarkers able to identify pathological changes to key structures in these networks are crucial, as they could have important implications for patient management and delivery of clinical interventions. Dopamine producing neurons are mainly located in the substantia nigra pars compacta (SNc) (Fig. 1) and ventral tegmental area (VTA),[1]

Received April 05, 2023. Revised July 17, 2023. Accepted August 20, 2023. Advance access publication September 5, 2023

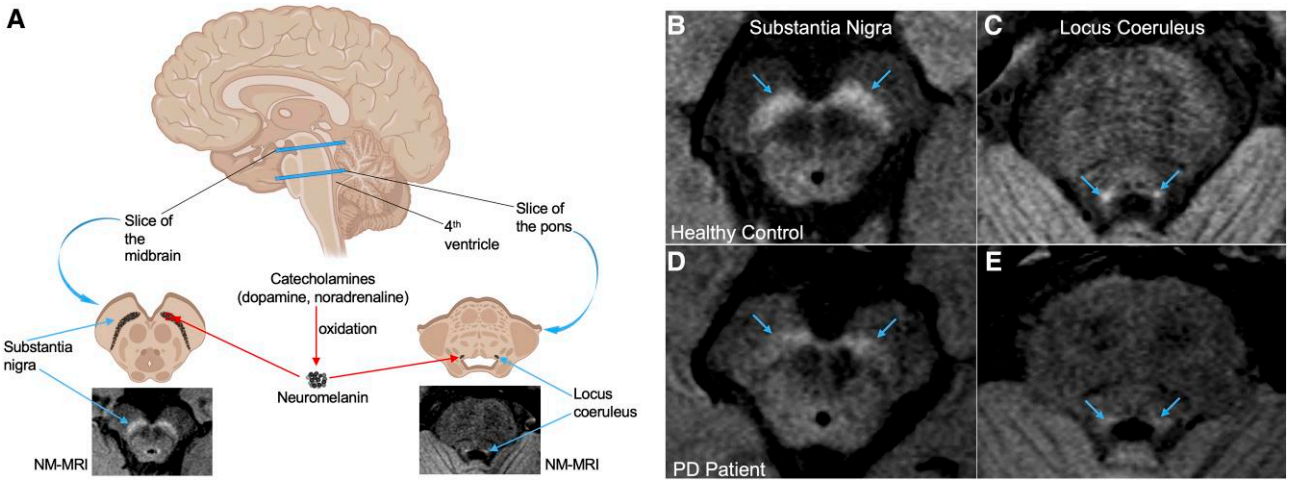

Figure 1 Anatomical localization of the substantia nigra and the locus coeruleus. (**A**) The dopamine producing neurons of the substantia nigra pars compacta (SNc) and ventral tegmental area (VTA) are located in the midbrain. The noradrenergic neurons of the locus coeruleus (LC) are localized in the upper dorsolateral pontine tegmentum bilateral to the fourth ventricle. The SNc-VTA and LC accumulate neuromelanin (NM), a dark pigment produced from catecholamine metabolism via iron-dependent oxidation. NM-MRI localizes in the SNc-VTA and LC as hyperintense regions (**B**–**E**). NM-MRI images at the levels of the SNc-VTA and LC for a healthy adult (65-year-old male) (**B** and **C**) and a patient with Parkinson's disease (71-year-old male) (**D** and **E**). Figure created with BioRender.com.

and dopaminergic signalling has been associated with modulation of behaviour and cognition, voluntary movement, motivation, punishment and reward, sleep, dreaming, mood, attention, working memory and learning.[2] The locus coeruleus (LC) (Fig. 1) contains the major proportion of noradrenergic cells, and it is involved in a variety of autonomic and cognitive functions, including working memory, learning and attention,[3-5] memory consolidation and retrieval,[6,7] arousal, REM sleep behaviour, pain modulation and stress response.[3,5,8] Given the critical role of the LC and SNc-VTA in neurodegenerative and psychiatric diseases, there is a considerable incentive to develop MRI techniques to assess the integrity of these structures *in vivo* with adequate sensitivity and specificity to guide differential diagnosis, quantify disease severity and offer insight into prognosis and treatment response.

Neuromelanin-sensitive magnetic resonance imaging (NM-MRI)[9] has shown accurate visualization of the SNc-VTA and LC, providing insights into the alterations of these structures and offering a non-invasive and cost-efficient way to investigate the human catecholamine function *in vivo*. NM-MRI allows the visualization of the SNc-VTA and LC due to the presence of neuromelanin (NM), a pigment that results from the oxidation of dopamine in the SNc-VTA, and noradrenaline in the LC, which serves as endogenous MRI contrast agent. NM normally accumulates with age, but it is relatively diminished in the SNc-VTA and LC of patients with neurodegenerative disorders.[10,11] Several NM-MRI research studies have shown significant reductions in measures of NM-MRI contrast and volume of the SNc-VTA and LC in patients with different neurological diseases, leading to the suggestion that the NM-related contrast in MRI images reflects a loss of NM-containing neurons.[12] In fact, direct comparisons between post-mortem NM-MRI and neuropathological findings[13-15] have shown that NM-MRI signal intensity in the SNc-VTA and LC is closely associated with the quantity of NM-containing neurons, supporting the link between NM-MRI hyperintensity with the presence of NM. Moreover, recent studies suggest that NM-MRI can also be used in non-neurodegenerative conditions, such as schizophrenia and drug abuse,[16] raising the prospect of NM-MRI being a potential biomarker for catecholamine function.[15,17-20]

While the number of studies using NM-MRI has grown substantially in the past decade, there are several limitations that need to be addressed before this technique is applied to clinical practice and can be used as a quantitative imaging biomarker. The main challenges are related to the clinical interpretation of the NM contrast, how contrast change relates to underlying pathology, and the need for a standardized protocol to aid in acquisition and data processing (a critical gap that prevents large-scale multisite studies and translation into the clinic). In this review article, we discuss the various biological and physical contrast mechanisms associated with NM-MRI, which are essential for the interpretation of the NM-MRI measures. We focus on the technical and practical aspects of the acquisition and image processing, providing valuable information for researchers aiming to optimize and standardize these methods. We review the potential clinical applications, and finally, we discuss some of the challenges and limitations and provide recommendations for future studies.

Contrast mechanisms associated with NM-MRI

Biological basis

Understanding the underlying biological correlates is crucial for the interpretation of NM-MRI measures and for the development of quantitative MRI-based *in vivo* biomarkers for LC and SNc-VTA integrity. The first publication proposing 'NM-sensitive MRI' found that the signal hyperintensities observed in a T1-weighted turbo spin echo sequence at 3 T corresponded well with the location of the LC and SNc-VTA in gross specimens.[9] They also observed that in patients with Parkinson's disease, the signal intensity in the LC and SNc-VTA was greatly reduced and concluded that reduced contrast in NM-MRI images reflects a loss of NM-containing neurons and/or decreased intracellular NM content. Since then, the number of studies using NM-MRI have grown exponentially and most of the studies associate the MR contrast to the presence of the NM pigment. NM is a polymeric pigment present in the human CNS produced from the catecholamine oxidation from the dopamine

precursor L-DOPA. NM normally accumulates with age in the SNc-VTA and LC, but it is relatively diminished in patients with known LC and SNc-VTA neurodegeneration. Several studies have uncovered a dual nature of NM that could be protective or toxic.[10,21] Intraneuronal NM can protect neurons in a couple of ways: during its biosynthesis, reactive catecholamines not accumulated in synaptic vesicles are removed from the cytosol[22] and it can bind toxins and redox active metals.[23] In contrast, NM released by dying neurons can contribute to the activation of microglia increasing neuroinflammation and neurodegeneration.[24] The NM pigment is composed of melanin, proteins, lipids and metal ions including iron, copper and zinc.[25] NM has two iron binding sites with different structure and affinity for the metal that result in unusual paramagnetic properties; it is measurable by electron spin resonance[26] and can also be detected using MRI.[10]

Direct comparisons between post-mortem NM-MRI and neuropathological findings have shown that NM-MRI signal intensities in the SNc-VTA[13] and LC[14] are closely associated with the quantity of NM-containing neurons, supporting the link between NM-MRI hyperintensity with the presence of NM. Recently, Cassidy and colleagues[15] validated that NM-MRI signal intensity in postmortem midbrain specimens correlated with regional NM concentration even in the absence of neurodegeneration. Moreover, using multimodal imaging (i.e. PET and MRI), they showed that the NM-MRI signal was related to both dopamine release in the dorsal striatum and resting blood flow within the SN. These recent studies suggest that in addition to the structural information provided by NM-MRI to localize the NM-containing structures, NM-MRI can also provide quantitative information about the NM concentration, which can be used as an indirect proxy for catecholamine function. This evidence suggests that NM-MRI can be used to investigate dopaminergic and noradrenergic function, even in the absence of neurodegeneration. In psychiatric disorders without catecholamine neuronal loss, NM-MRI may reflect catecholamine dysfunction.[16] In conditions such as psychosis and schizophrenia, augmented synthesis of dopamine in the SNc-VTA results in increased NM concentration[27] which has been associated with increased NM-MRI signal.[15,28,29]

Conversely, recent studies focused on *in vivo* imaging of the noradrenergic neurons of the LC have challenged the concept that the contrast in NM-MRI is produced by the presence of NM. These studies propose that the main source of the high signal intensity in NM-MRI is not the presence of T1-shortening paramagnetic molecules like NM, but the higher water content in the noradrenergic neurons.[30-32] This hypothesis was supported by *in vivo* experiments with young and transgenic rodent models.[31] They observed an absence of a high MRI signal from the LC of *Ear2*$^{-/-}$ mice lacking noradrenergic neurons and suggested that cell bodies of noradrenergic neurons are the source of high MR signal intensity. Furthermore, they observed the high signal in the LC in *Dbh*$^{-/-}$ mice and in 3-week-old mice, both of whom lack NM and concluded that the MR contrast is not due to NM, dopamine β-hydroxylase, or their binding to paramagnetic ions, blood inflow or haemoglobin, and instead suggested that the high density of water protons as the relevant source of the high MRI signal. This hypothesis has also been supported by a recent study aiming to unravel the contributions of the NM-MRI contrast which suggested that the NM-MRI contrast is associated with a lower macromolecular fraction in the LC (i.e. ratio between macromolecules and water protons).[33] These findings have led to recent discussions on whether the neuroimaging community should continue to use the term 'Neuromelanin-sensitive MRI', as the enhanced contrast in the SNc-VTA and LC is associated with the properties of the NM-containing neurons and not necessarily caused by the direct presence of NM.[34,35]

Lastly, given the long acquisition times, most of the studies using NM-MRI have used a reduced field-of-view covering just the brainstem. In this section, the structures containing high levels of NM (i.e. SNc-VTA and LC) show signal hyperintensities relative to other tissues. However, if the field-of-view is extended to cover other regions, it is possible that similar hyperintensities may be evident in structures that do not contain high levels of NM (e.g. striatum), and future studies should investigate this aspect to assess the specificity of NM-MRI to NM concentration.

Physical basis

The first study describing the NM-MRI technique[9] suggested that the source of the hyperintensity was paramagnetic T1-shortening effects associated with the presence of NM. This idea has been supported by *in vitro* studies showing that the NM-iron complex produces concentration-dependent T1 shortening effects.[36-39] However, it has also been reported that T1 values alone cannot account for the contrast seen in NM-MRI images,[40,41] and therefore other mechanisms must contribute to the contrast.

Observations that magnetization transfer (MT) preparation of NM-MRI pulse sequences increases contrast between the SNc-VTA and surrounding brain tissue has led several authors to credit MT as the primary source of contrast.[40,42,43] NM-MRI was originally based on a two-dimensional T1-weighted turbo spin-echo (TSE) pulse sequence,[9] which is sensitive to intrinsic MT effects.[44] Moreover, different studies have shown that explicit MT preparation of different pulse sequences (including TSE, 2D and 3D gradient echo (GRE) sequences) increases the contrast between the NM-containing structures and surrounding brain tissues, and therefore it is likely that MT is a primary source of NM-MRI contrast.[40,42] Furthermore, recent studies of the LC using MT-weighted images at 7 T showed that the LC contrast is enhanced by applying MT preparation and suggested that MT-weighted sequences are the most appropriate method for visualizing the LC at 7 T.[45,46]

MT contrast is generated by the interaction between mobile water protons and the protons associated with tissue macromolecules (i.e. protons bound to immobile proteins, large macromolecules, or cellular membranes).[47] Given substantial variation between macromolecular compositions of tissues, this interaction differs by tissue type and results in macromolecular-sensitive contrast in MT-weighted images. In NM-MRI, applying the MT preparation improves the observable contrast of the SNc-VTA and LC (Fig. 2), by providing higher saturation to adjacent tissues (due to higher macromolecular content) and leaving the SNc-VTA and LC relatively hyperintense.

The NM-MRI contrast may be the product of a combination of MT and T1 effects, similar to MT-based background suppression in MR angiography.[48] This hypothesis has been supported by *in vivo* studies using quantitative MT (qMT) methods that provide quantitative indices of tissue structure, such as the macromolecular-to-free water pool size ratio (PSR). These studies showed that the SN[49,50] and LC[51] have lower PSR compared to surrounding tissues. Low PSR indicates low macromolecular content and/or high free water content, which is consistent with recent publications[30,31,33] that suggest that the high signal intensities in the LC are related to the higher density of water protons. As described in the previous section 'Biological basis', Watanabe and colleagues[30,31] performed *in vivo* experiments in humans and transgenic rodents that

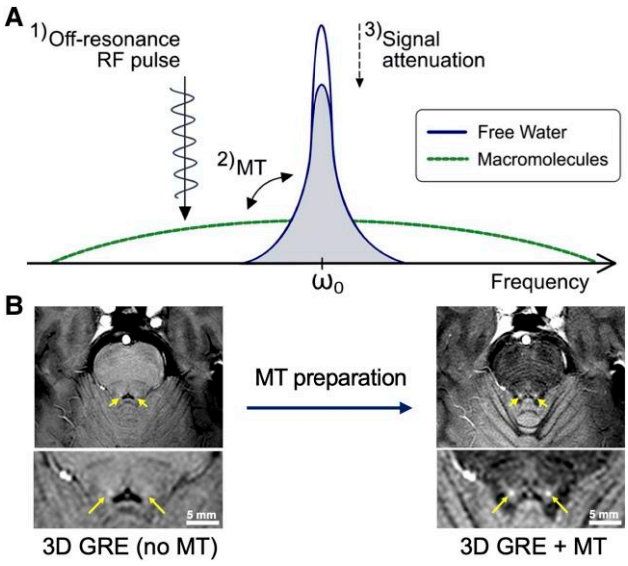

Figure 2 Magnetization transfer effect. (**A**) The water pool has a narrow spectrum, while the macromolecular pool has a broadened line. When a radiofrequency (RF) pulse is applied off-resonance (1), it will selectively saturate the macromolecular protons without directly affecting the free water protons. This saturation is then transferred to the water protons (2), resulting in an observed signal attenuation (3). ω_0 = water resonance frequency. (**B**) Example of a 3D gradient echo (GRE) image without (*left*) and with magnetization transfer (MT) preparation at the level of the locus coeruleus (arrows).

provided evidence to support the hypothesis that source of the high MRI signal is not NM, but the higher density of water protons whose T1 is shortened by paramagnetic ions.

In conclusion, the SN and LC hyperintensities are the result of the combination of low PSR (i.e. lower macromolecular content/higher free water content) and the shorter T1 relative to other grey matter structures (possibly due to the presence of NM and other metal ions). The combination of T1-weighted imaging (present in both TSE and GRE sequences) and MT-preparation results in saturation of white matter (due to higher PSR) and grey matter structures adjacent to the SN and LC (due to higher PSR and/or longer T1) leaving these two structures relatively hyperintense.

NM-MRI acquisition

MRI sequence

TSE sequences with explicit MT contrast preparation pulse have shown higher sensitivity in detecting NM containing structures in the brain than those relying on incidental MT effects.[40,42,43,50] Other studies have extended this result by applying explicit MT preparation pulses to 2D and 3D GRE pulse sequences to establish contrast between NM-containing structures and their surroundings.[43,50,52-54] Table 1 summarizes the ranges for the main acquisition parameters for the mostly used TSE, 2D GRE and 3D GRE sequences. Typical acquisition times vary between 5 and 10 min depending on the coverage (i.e. number of slices and thickness), number of averages (typically three to eight) and fast imaging options (e.g. SENSE, GRAPPA, TSE factor). Figure 3 shows an example of NM-MRI images acquired with typical TSE, 2D GRE and 3D GRE sequences.

To date, most of the NM-MRI studies have used a TSE sequence at 3 T. Although TSE sequences are relatively easy to implement in clinical scanners from different manufactures, they have several limitations. In a multi-slice TSE sequence, the slice selective excitation and refocusing pulses of one slice act as off-resonance pulses for neighbouring slices, leading to increased MT effects on signal intensity. However, the combination of refocusing and explicit MT pre-pulses can cause specific absorption rate (SAR) to impose limitations on the scan. If the protocol delivers SAR values higher than the safety limit, the MRI scanner may force modifications in scan parameters to reduce the SAR (such as changes in field-of-view, number of slices, resolution, lengthening repetition time or reducing the echo train length). Changes in acquisition parameters may limit the reproducibility of NM-MRI by adding confounding factors. Moreover, the signal intensity obtained from 2D TSE is not homogeneous across slices due to the sensitivity to the radiofrequency (B_1) field, and 2D TSE acquisitions frequently require a space gap between slices. Finally, individual high resolution in-plane NM-MRI acquired with TSE sequences have low signal to noise ratio (SNR) and low contrast-to-noise ratio (CNR), and therefore a multiple number of signal averages/acquisitions (NSA) and/or thicker slice thickness (2–3 mm) are needed to compensate for lower SNR in these sequences at the cost of partial-volume effects and increased scanning times.

GRE sequences can overcome some of the limitations of the TSE sequences and have advantages in terms of resolution and scan-time. Different studies have shown that GRE sequences with MT pre-pulse produce similar or even higher SN and LC contrast to those using the TSE with MT preparation.[15,43,49-53,55] These sequences deposit a lower level of SAR without compromising contrast sensitivity.[53] Given the lower SAR in GRE sequences compared to TSE, these sequences are also more feasible to implement at 7 T[45,46] to take advantage of the greater SNR at higher field.

Sequence optimization

The contrast in NM-MRI images can be enhanced by the choosing the optimal combination of imaging parameters. Since the magnitude of MT effect depends on the offset frequency and power (i.e. shape, amplitude and duration) of the MT preparation pulse, optimizing NM-MRI contrast should benefit from examining the MT effect of relevant tissues and adjusting the MT pulse to provide the best SNc-VTA and LC contrast. It has been shown an MT pre-pulse at a frequency offset in the range 1000–2000Hz provides greatest SN and LC contrast.[45,50] Other key variables in the MT-prepared GRE sequences are the repetition time (TR), echo time (TE) and flip angle (FA). The minimum TR is generally limited by the power delivered by the MT pre-pulse. The FA can be optimized, and a recent study investigating the NM contrast in the SN and LC as a function of the FA using a 3D GRE approach found that the FA that provided the best NM contrast was 15°–20° for the SNc-VTA and 20°–25° for the LC.[56]

The choice of MRI pulse sequence may also affect sensitivity to motion artefacts, with 3D acquisitions being generally more prone to motion artefacts compared to 2D acquisitions. Regardless of the type of sequence used, it is recommended to use thin pillows on the base of the coil to ensure tight fixation and minimize motion. Moreover, to correct for possible head motion during long NM-MRI scans, the multiple acquisitions should be individually saved for offline motion correction before averaging (i.e. online averaging of the images should be avoided). Using this approach, the individual images with severe motion artefacts can be discarded and head motion across measurements can be partly corrected.[53]

Table 1 Typical acquisition parameters for neuromelanin (NM)-MRI based on turbo spin echo (TSE), 2D gradient echo (GRE) and 3D GRE sequences

Sequence	TR (ms)	TE (ms)	FA (degrees)	In-plane resolution	Slice thickness
TSE	500–1000	9–15	90	0.4×0.4–0.8×0.8 mm^2	2–3 mm
2D GRE	260–500	2–6.5	40–60	0.4×0.4–0.7×0.7 mm^2	1.5–3 mm
3D GRE	26–62	2–8	12–30	0.4×0.4–1.5×1.5 mm^2	0.7–2 mm

FA = flip angle; TE = echo time; TR = repetition time.

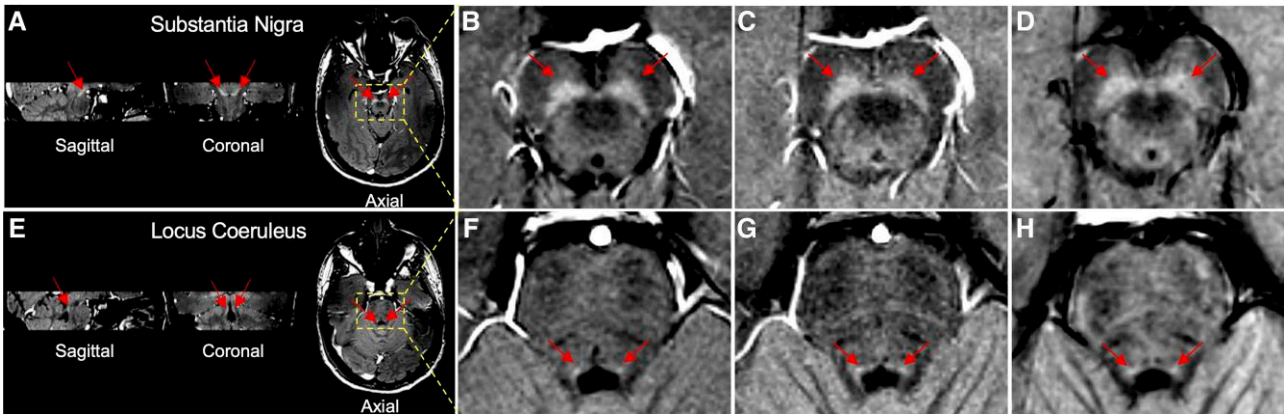

Figure 3 Representative neuromelanin (NM)-MRI images acquired with typical 3D gradient echo (GRE), 2D GRE and turbo spin-echo (TSE) sequences. (**A** and **E**) Sagittal, coronal and axial reconstructions of 3D GRE NM-MRI showing the location of the substantia nigra (SN) (*top*) and locus coeruleus (LC) (*bottom*). (**B** and **F**) 3D GRE sequence [repetition time (TR)/echo time (TE) = 25/2.9 ms, flip angle = 16, field of view (FOV) = 210 × 170, resolution = 0.6 × 0.6, slice thickness = 1, 45 slices, magnetization transfer (MT) pulse: single-lobed sinc-gauss pulse, duration = 11 ms, offset frequency = 2000 Hz, αMT = 480°; four acquisitions, total scan duration = 6:58 min]. (**C** and **G**) 2D GRE sequence (TR/TE = 420/6.1 ms, flip angle = 60, FOV = 210 × 170, resolution = 0.6 × 0.6, slice thickness = 3, 15 slices, MT pulse: single-lobed sinc-gauss pulse, duration = 11 ms, offset frequency = 2000 Hz, αMT = 480°; four acquisitions, total scan duration = 8:00 min). (**D** and **H**) TSE sequence (TR/TE = 670/12 ms, flip angle = 90, FOV = 210 × 170, resolution = 0.6 × 0.6, slice thickness = 3, 15 slices, TSE factor = 8, MT pulse: single-lobed sinc-gauss pulse, duration = 23 ms, offset frequency = 2000 Hz, αMT = 600°; four acquisitions, total scan duration = 6:10 min). All images were acquired from the same healthy participant (24-year-old male) as oblique slices covering the midbrain and pons oriented perpendicular to the floor of the fourth ventricle.

Image resolution

An important aspect of the NM-MRI acquisition is the image resolution. The small sizes of the SNc-VTA and, particularly the LC (~15 mm in length and 1–3 mm in diameter), have motivated the use of high-resolution at the cost of relatively low SNR and low CNR and higher vulnerability to motion. High in-plane resolution (~0.4×0.4 mm^2) and thick slices (~2–3 mm) (resulting in anisotropic voxels) have been used in 2D TSE and 2D GRE sequences to increase the SNR and reduce scan times. However, this strategy is prone to partial volume effects (i.e. inclusion of non SNc-VTA and LC tissue within a voxel), particularly at the most rostral and caudal aspects of the SNc-VTA and LC, leading to biases in segmentation.[57] Alternatively, more isotropic voxels (e.g. 0.75 mm × 0.75 mm × 0.75 mm at 3 T[58]) obtained with 3D sequences[45,51,52,58] can be used to capture the rostro-caudal distribution of SNc-VTA and LC signal intensity and allow for more accurate segmentation and volumetric measures.

Positioning of the field-of-view

Another strategy to reduce scan times is to decrease the size of the field-of-view to comprise the brainstem only. However, template-based segmentation approaches (see the 'Definition of the regions-of-interest' section) are more challenging with reduced field-of-view acquisitions. Moreover, the reduced field-of-view in the inferior-superior direction covering just the midbrain and upper pons may result in the potential loss of data from the accidental exclusion of parts of the SNc-VTA and LC, and therefore the positioning of the field-of-view is critical. Most studies have placed the field-of-view perpendicular to the floor of the fourth ventricle (Fig. 4B), while others have placed the field-of-view along the anterior commissure-posterior commissure (AC-PC) line[15,59] (Fig. 4C). While the volume placement perpendicular to the floor of the fourth ventricle may provide less partial volume effects than AC-PC alignment, the AC-PC line is a clearly defined landmark, and this alignment was shown to provide excellent reproducibility and test-retest reliability.[55] Recently, Wengler and colleagues proposed a detailed NM-MRI volume placement procedure based on distinct anatomical landmarks to improve within-subject and across-subject repeatability and reproducibility, and recommended quality control checks to ensure usable data, providing a foundation for the optimization and standardization of NM-MRI.[55,60]

Left–right asymmetries

Finally, some studies have reported left/right asymmetries in the NM-MRI contrast. Studies using Philips scanners have observed higher LC contrast on the right side,[51,61] while other studies using 3 T Siemens scanners have shown opposite asymmetry,[58,62] suggesting that the asymmetry is not related to biological left/right differences, and that there could be a bias introduced by the direction

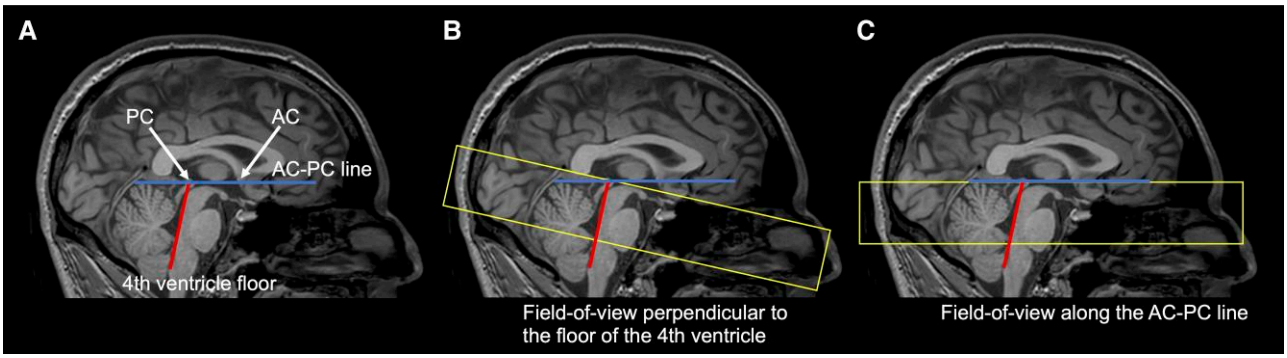

Figure 4 Typical placement of the field-of-view in neuromelanin (NM)-MRI acquisitions. (**A**) Sagittal T1-weighted image showing the anterior commissure-posterior commissure (AC-PC) line (blue line) and the floor of the fourth ventricle (red line). (**B**) Field of view (yellow box) positioned with the transverse slices oriented perpendicular to floor of the fourth ventricle. (**C**) Field of view (yellow box) positioned with the transverse slices were oriented along the AC-PC line. The field of view in **B** and **C** have the same size and cover both the substantia nigra (SN) and locus coeruleus (LC), but the orientation of the transverse slices is different.

of the magnetic field. These asymmetries could also be related to B_1 field variations, and future NM-MRI imaging studies should investigate this issue further and incorporate field corrections.

In conclusion, NM-MRI is critically dependent on the acquisition sequence and parameters. Future studies should evaluate the optimal combination of imaging parameters (i.e. power and frequency offset of the MT-pulse, repetition time (TR), echo time (TE), flip angle, size and placement of the field-of-view, in-plane resolution, slice thickness and minimum number of signal averages). It is essential to reach expert consensus on technical guidelines for the image acquisition. This will allow multicenter data collection and lead to a better validation of NM-MRI as an effective biomarker.

NM-MRI image analysis

Definition of the regions-of-interest

Most of the studies using NM-MRI have performed the image analyses in subject space. The first step in processing the NM-MRI images is the identification of the regions-of-interest (ROI) for the SNc-VTA and LC. In most studies, the SNc-VTA complex is segmented together as it is difficult to define the border between SNc and VTA, and most authors refer to this region as simply SN or SNc. For the SNc-VTA segmentation, several studies have used a manual contour drawing of the SNc-VTA based on the observed signal hyperintensity (Fig. 5A)[63-69] which is thus subject to operator bias, low reproducibility and a significant amount of manual work. Other studies have defined ROIs in subregions of the SN using circular cursors at locations of the lateral, central and medial parts of the SN (Fig. 5B).[70-75] Others have proposed automatic/semi-automatic methods to delineate the SNc-VTA (Fig. 5C and D).[52,54,76-81] Recently, atlas-based segmentation[82,83] and deep learning methods[84-86] have been proposed as promising approaches to account for the inter-subject and inter-operator variability.

The small size of the LC and its position close to the fourth ventricle make segmentation more challenging. In some studies, the LC has been identified manually,[9,54,70,71,74] while others employed semi-automated[51,53,80,87-89] (Fig. 5E–J) and automated[76] methods. Keren and colleagues[90] proposed a probabilistic map of the LC in standard Montreal Neurological Institute (MNI) coordinate space and several studies have used these coordinates to identify the location of the LC.[91] Semi-automated LC segmentation can also be performed through the creation of group-average NM-MRI templates where the LC can be easily identified.[58,62] The resulting LC ROI can then be spatially transformed to subject space using accurate co-registration. Recently, a study using high-resolution ($0.4 \times 0.4 \times 0.5$ mm) MT-weighted images at ultrahigh field 7 T MRI proposed a probabilistic LC atlas for older adults.[92] The contrast and variance along the LC atlas mirrored distinctive *ex vivo* spatial distributions of LC cells in its subregions. Using accurate co-registration, this atlas can be transformed to each subject's native space to facilitate accurate LC localization in future studies.

Quantitative measures

MRI studies with NM-MRI sequences have consistently demonstrated the presence of a significant reduction of NM-related signal in the SN (SNc-VTA) and LC in patients with neurodegenerative conditions compared to age-matched healthy controls. To quantify these signal reductions, different studies have used various outcome measures such as SN area, SN volume, SN width and SN (and LC) contrast ratio to a reference adjacent tissue (Fig. 6).

The area of the SN has been generally obtained from 2D TSE images and has been manually traced or defined by the number of voxels in the mesencephalic region with signal intensity values higher than a specified threshold in one or two slices.[54,77,93-98] This measure, however, is critically dependent on the selected slice (or slices) which can vary between subjects and, given the slice thickness used in 2D TSE sequences (2–3 mm), is prone to partial volume effects. In addition to the SN area, some studies have also used manual width measurements to investigate pattern changes in the different segments of the SN.[94,99-102]

SN volume measures have been obtained from 2D and 3D images. The SN has been defined manually,[63,65-67,69,103,104] semi-automatically,[52,81,105] or automatically[76] in multiple slices where the SN hyperintensity is observed, and the volume is calculated as the number of voxels multiplied by voxel size (i.e. in-plane resolution and slice thickness). SN volume measures have also several limitations since most of the reports used a 2D TSE sequence which is prone to partial volume effects and signal inhomogeneities across slices. Moreover, the volume measures from manually defined SN provide subjective measures. 3D sequences that use more isotropic voxels and automatic SN segmentation approaches should provide more accurate (and less subjective) volumetric measures.[52]

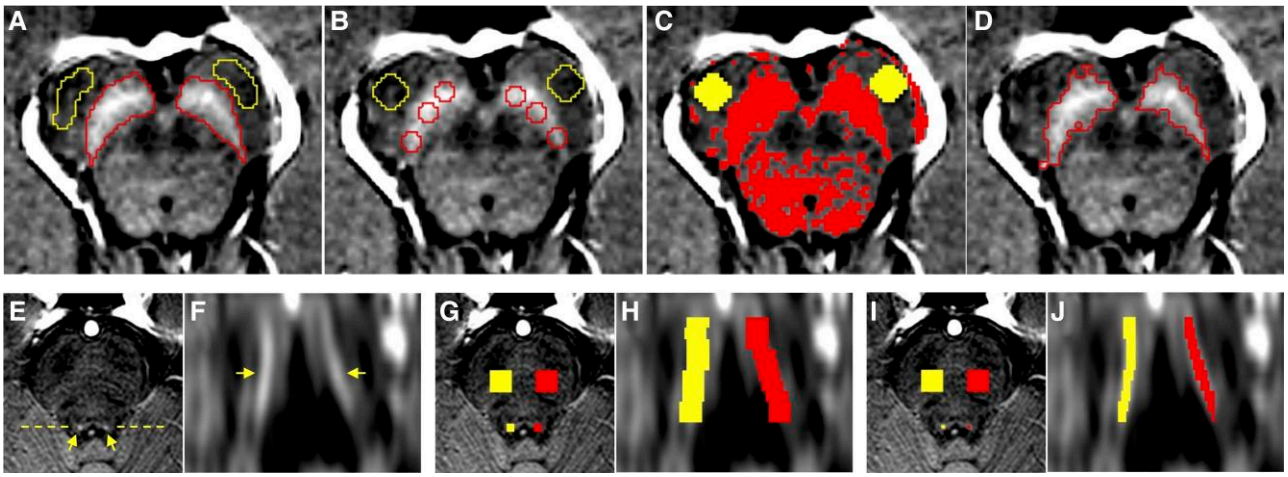

Figure 5 Definition of the regions of interest for the substantia nigra pars compacta-ventral tegmental area (SNc-VTA) and locus coeruleus (LC). (**A**) Manual definition of the SNc-VTA (red) and refence region in the cerebral crus (CC) (yellow) based on observed signal intensity. (**B**) Reference region (yellow) and subregions of the SN (red) using circular cursors at locations of the lateral, central and medial parts of the SN. (**C–D**) Semiautomatic definition SNc-VTA: (**C**) The CC region (yellow) is defined on each side on each slice where the SNc-VTA is visible; then for each slice, a binary map is defined as the voxels in the mesencephalic region with signal intensity greater than $MN_{CC} + 3{\times}SD_{CC}$, where MN_{CC} and SD_{CC} are the mean and standard deviation for the background region of interest (ROI) located in the cerebral crus on the corresponding slice and side. (**D**) Finally, the ROIs for the SN are then defined on the binary map. (**E–J**) Semiautomatic definition of the region of interest for the LC: (**E**) Axial view of the pons; the dashed line indicates the level of the coronal view shown in **F**, and the arrows indicate the location of the LC. (**F**) Coronal view of the LC (arrows). (**G**) Initial ROIs around the LC and reference ROIs in the on the left (red) and right (yellow) sides; (**H**) Coronal view of the initial LC ROIs. (**I–J**) Final LC ROI consisting of the contiguous voxels (for each slice and side) with the highest signal intensity within the initial ROI.

Most of the NM-MRI studies have normalized the SN (and LC) signal intensity to that of a neighbouring reference region to calculate the contrast ratio (CR). The great majority use CR calculated as $CR = (S_{SN} - S_{ref}) / S_{ref}$, where S_{SN} represents the mean signal intensity of the SN and S_{ref} the mean signal intensity of a reference region, generally in the cerebral crus (CC). The same formulation has also been referred to as magnetization transfer contrast (MTC)[80] or contrast-to-noise ratio (CNR).[106] Additionally, one study calculated CR as $CR = S_{SN} / S_{ref}$,[54] and other studies calculated CNR as follows: $CNR = (SI_{SN} - SI_{ref}) / SD_{ref}$, where SI represents mean signal intensity and SD_{ref} is the standard deviation of the signal in the reference region.[53,81] Similar measures have been used to calculate the CR of the LC relative to a reference region, generally located in the pontine tegmentum. Generally, the CR measures are obtained for each slice and each side separately and then averaged to obtain a global measure. While the CR shows differences between patients and controls, this approach also has several limitations. In most cases, it does not examine the entire SN, but only one or few slices, and there is variability for the location and orientation of these slices. There is also variability in the location and size of the reference regions. Moreover, as described in the previous section, the SN is generally segmented using manual, semi-automatic and automatic methods that depend on the SN signal hyperintensity. In patient populations, there is signal loss in the SNc-VTA and LC, and therefore the borders of these structures are difficult to define. This may bias the analysis by excluding impacted portions of the SNc-VTA and LC that have decreased signal, and therefore valuable information about affected regions is lost. This results in an overestimation of the CR in patients that is the direct result of the CR reliance on ROI definition.

Voxel-wise analyses

Some studies have obtained the CR for subregions for the SN to investigate the progression of the neurodegenerative process within the SN[70-75,102,107,108] which is not uniform throughout the structure. To obtain a more detailed assessment of the subregional variation on NM-MRI signal within the SNc-VTA, recent studies have proposed voxel-wise analyses to capture fine-grained anatomical information and identify the subregions most affected by pathology[15,29,59] (Fig. 7). In these approaches, the NM-MRI images are normalized to a standard space, and the ROIs are defined from a NM-MRI template obtained from the average of a large dataset avoiding the bias from defining the ROIs based on each-subject's images. The CR is calculated for each voxel in the SNc-VTA ROI as $CR = (I_{SN} - Mode(I_{ref})) / Mode(I_{ref})$, where I_{SN} represents the signal intensity of each voxel in the SNc-VTA and $Mode(I_{ref})$ is the mode of the signal intensity of the reference region in the CC, as the mode has been shown to be more robust to outlier voxels than the mean or median. The voxel-wise methods are fully automated and require only a few minutes to conduct, minimizing impediments to its wide-scale use as a routine clinical and screening tool.

Harmonization

The optimization of NM-MRI as a generalizable biomarker for catecholamine function requires large-scale samples demanding harmonization approaches to combine data collected from multiple sites. However, combining MRI data from multiple sites can introduce non-biological variability from differences in image acquisition related to hardware (e.g. MRI scanner vendor or head coil) or software (e.g. pulse sequence parameters). Recently, Wengler and colleagues[109] have proposed a method to harmonize NM-MRI data to effectively remove non-biological variability while maintaining biologically relevant variability (e.g. associated with age). This method has produced improvements in statistical power and reproducibility facilitating large-scale multisite studies to develop NM-MRI-based biomarkers.

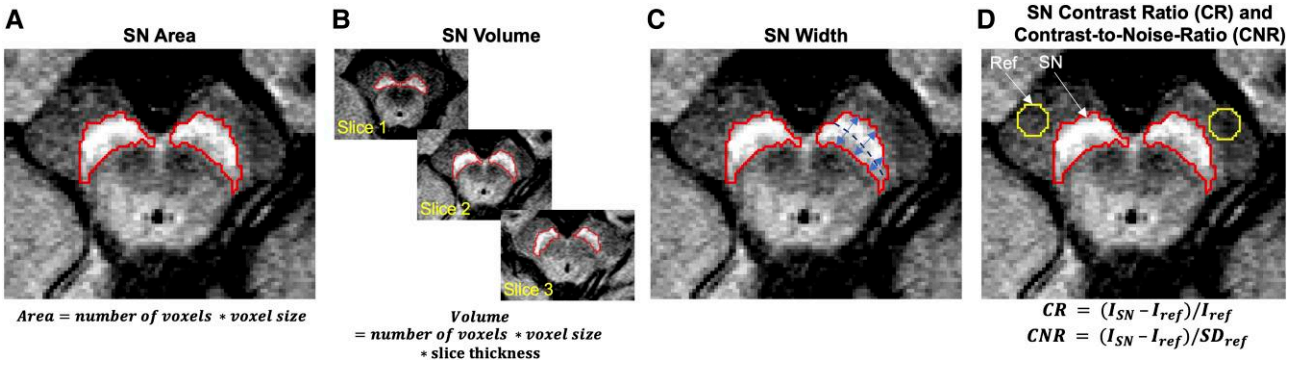

Figure 6 Neuromelanin (NM)-MRI outcome measures. (**A**) The area of the substantia nigra (SN) is defined by the number of voxels in the mesencephalic region with signal intensity values higher than a specified threshold in one or two slices. (**B**) The SN is defined manually, semi-automatically or automatically in multiple slices where the SN hyperintensity is observed, and the volume is calculated as the number of voxels multiplied by voxel size (i.e. in-plane resolution and slice thickness). (**C**) The length line is defined following the maximal longitudinal length of the SN area and is divided into three equal segments defining the lateral, central and medial parts of the SN. The maximal width of each part of the SN is measured perpendicular to the length line. (**D**) The contrast ratio (CR) is calculated as $CR = (S_{SN} - S_{ref}) / S_{ref}$, where S_{SN} represents the mean signal intensity of the SN and S_{ref} the mean signal intensity of a reference region, generally in the cerebral crus; other studies calculate the contrast-to-noise ratio (CNR) as $CNR = (SI_{SN} - SI_{ref}) / SD_{ref}$, where SI represents mean signal intensity and SD_{ref} is the standard deviation of the signal in the reference region.

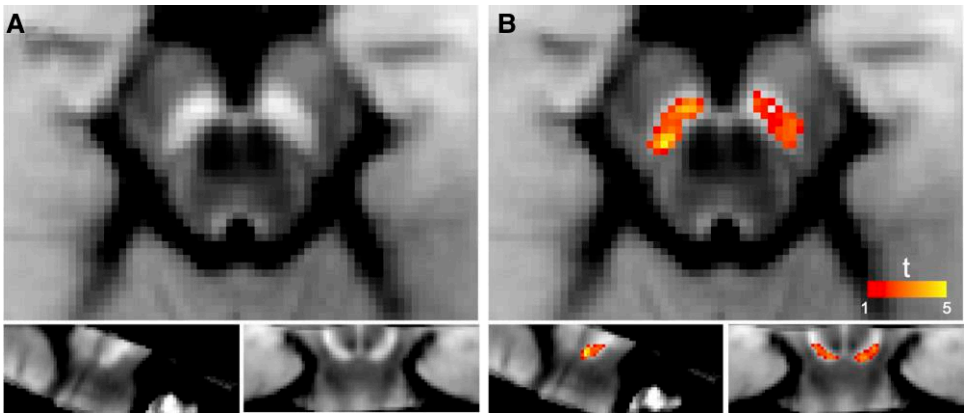

Figure 7 Example of voxel-wise analysis. (**A**) Template neuromelanin (NM)-MRI image created by averaging the spatially normalized NM-MRI images from 30 individuals in Montreal Neurological Institute (MNI) space (*top*: axial, *bottom left*: sagittal, *bottom right*: coronal). (**B**) Map of substantia nigra pars compacta-ventral tegmental area (SNc-VTA) voxels, where NM-MRI contrast ratio was different between Parkinson's disease patients and age-matched healthy controls (thresholded at $P < 0.05$, voxel level) overlaid on the NM-MRI template.

Potential clinical applications of NM-MRI in neurological and psychiatric disorders

Parkinson's disease

NM-MRI shows that the volume and contrast ratio (CR) of the SNc-VTA and LC are decreased in Parkinson's disease patients compared to healthy controls (Fig. 1) with good sensitivity and specificity.[110,111] NM-MRI signal is decreased even in early and pre-symptomatic stages of Parkinson's disease[112-114] and diminishes with disease duration and severity.[9,54,74,75,81,115] NM-MRI shows reductions in the SNc-VTA that progress from the lateral to central and medial regions.[102,116] Longitudinal studies found reductions in the total volume and CR of the SNc of Parkinson's disease patients over the course of 2–3 years.[68,75,117] Furthermore, NM-MRI measures have been associated with motor[69,118-120] and non-motor symptoms.[116,121-123]

Parkinson's 'plus' disorders

NM-MRI is also useful in detecting SNc and LC changes in other parkinsonian disorders, including multiple system atrophy, progressive supranuclear palsy and corticobasal degeneration, for which early-stage discrimination can be difficult.[66] NM-MRI has been shown to detect differences in signal intensity in both the lateral SNc and LC among multiple system atrophy, progressive supranuclear palsy and Parkinson's disease in their early stages.[75] The signal in the NM-sensitive area of the SNc has been shown to be lower in progressive supranuclear palsy than in Parkinson's disease patients.[98] The NM-MRI CR in the LC has also been shown to be significantly lower in progressive supranuclear palsy compared to Parkinson's disease,[124] and it has been suggested that NM-based SNc volume serves to differentiate progressive supranuclear palsy from Parkinson's disease,[125] indicating that NM-MRI could potentially be used as diagnostic tool to differentiate parkinsonisms.

REM sleep behaviour disorder

NM-MRI has also proven useful in mapping spatiotemporal changes in patients with REM sleep behaviour disorder (RBD).[116,126,127] Patients with RBD have a highly increased risk of later developing Parkinson's disease, dementia with Lewy bodies, multiple system atrophy and mild cognitive impairment.[128-130] NM-MRI studies investigating RBD patients showed a reduction in

NM-sensitive volume and signal intensity in the SNc-VTA compared to controls,[86,104] and SNc-VTA volume loss was equal to or lower than those with Parkinson's disease.[86,116] NM-sensitive signal changes first appear along the posterolateral motor areas of the SNc and then progress to more medial areas.[116] RBD is also associated with LC dysfunction,[88,89,131] and LC NM-imaging could potentially be used as a biomarker in patients at risk of developing neurogenerative conditions.

Alzheimer's disease

The LC undergoes significant neuronal loss in patients with Alzheimer's disease, which correlates with both disease severity and duration.[132-135] Neuronal loss is most evident in the rostral and middle portions of the LC, and volume loss across the LC aligns with Braak staging.[134,136-138] Updated Braak staging methods suggest that in Braak stage I, roughly 15% of LC neurons are tau positive,[139] and those positive cells have significant reductions in synaptic connectivity.[140,141] NM-MRI CR in the LC is reduced in Alzheimer's disease patients compared to age-matched controls, and it is significantly correlated with cognitive decline and disease severity.[142-144]

Psychiatric disorders: depression, schizophrenia and drug addiction

NM-containing structures have also been implicated in a variety of psychiatric disorders. In schizophrenia, the CR of the SNc has been shown to be significantly elevated compared to controls.[145,146] In patients with depression, the CR in the LC is significantly lower in the rostral and middle portions compared to controls.[147,148] Compared with control subjects, cocaine users show significantly increased NM-MRI signal in ventrolateral regions of the SN.[29] These findings suggest that in addition to its use as a marker of neuronal loss in neurodegenerative conditions, NM-MRI could possibly also be used as a marker of catecholamine function in a variety of psychiatric research.[16,29,59,149,150]

Ageing

In healthy subjects, the NM signal in the LC shows an inverted U-shape, in which the signal increases until approximately age 60 and then slowly decreases as subjects continue to age.[9,62,151] The same inverted U-shape was found for NM signal in the SNc-VTA, although the peak tends to be closer to 50 years of age and declines slowly after.[152] NM-MRI has also recently been used to associate LC integrity and cognition, showing that in a large cohort of older males (aged 62–71), lower LC integrity is associated with poorer episodic memory, general verbal fluency and processing speed, as well as increased odds of amnestic mild cognitive impairment (aMCI) daytime dysfunction.[153]

NM-MRI as a quantitative imaging biomarker

A biomarker has been defined as 'a characteristic that is objectively measured and evaluated as an indicator of normal biological processes, pathogenic processes or pharmacologic responses to a therapeutic intervention'.[154] A biomarker can be used for diagnosis, prognosis, staging or prediction and monitoring of the clinical response of a disease to a therapeutic intervention. Extending this concept, a quantitative imaging biomarker is an objective characteristic derived from an *in vivo* image measured on a ratio or interval scale as an indicator of normal biological processes, pathogenic processes or a response to a therapeutic intervention. Quantitative imaging biomarkers are sensitive, specific, accurate and reproducible imaging measures of biological processes that can be used in disease diagnosis, treatment planning and new therapeutic development, should provide clinically relevant information, and be validated by demonstrating the association between the measured biomarker value and a physiologic, pathophysiologic or therapeutic response. While there is a growing body of evidence that NM-MRI can be useful in the detection and monitoring of different neurodegenerative and psychiatric diseases, NM-MRI does not yet have the validation necessary to be considered a quantitative imaging biomarker, and it is not ready to be incorporated into routine clinical practice or therapeutic trials. It is insufficiently supported by histological correlation studies, and only a few studies have evaluated the sensitivity, specificity, accuracy and reproducibility of this technique.

Systematic reviews and meta-analyses have shown good diagnostic performance of NM-MRI for differentiating patients with Parkinson's disease from healthy controls. The first meta-analysis showed a pooled sensitivity of 0.82% [95% confidence interval (CI), 0.74–0.87] and a pooled specificity of 0.82 (95% CI, 0.73–0.89),[111] while a second more recent meta-analysis that included newer studies and increased the number of individuals showed a pooled sensitivity of 0.89 (95% CI, 0.86–0.92) and a similar pooled specificity of 0.83 (95% CI, 0.76–0.88). The authors concluded that NM-MRI provides a valuable tool for the diagnosis of Parkinson's disease, but given the large variability in the methods used by the different studies in terms of image acquisition and measurements, they recommended NM-MRI protocol standardization and large-scale multi-site validation. Another recent meta-analysis performed a quantitative synthesis of studies investigating NM-MRI in schizophrenia,[145] and the results showed that the NM-MRI CR in the SN were significantly higher in patients with schizophrenia compared to controls, but the study did not present data regarding sensitivity, specificity and accuracy. The authors concluded that NM-MRI is a candidate biomarker for dopamine dysfunction in schizophrenia, but further studies are needed to assess this marker in large, longitudinal cohorts and address potential effects of disease state, medication and correlations with symptoms.

A common conclusion from most of the studies using NM-MRI is that this method is a promising tool but requires further validation and development of harmonization protocols to facilitate large-scale multisite studies necessary for biomarker development. The search for imaging biomarkers is an active and promising field of research, and the interest in NM-MRI continues to increase, which is evident by the number of publications using NM-MRI. Given the promising results from the growing number of studies, we consider that NM-MRI has the potential to become a biomarker of dopaminergic and noradrenergic function in neurodegenerative and psychiatric disorders, but further efforts are necessary to establish NM-MRI as a biomarker. Much remains to be done to validate NM-MRI against histopathological data, assess the correlation with clinical status and disease progression, and determine the sensitivity, specificity and reproducibility of this method. In the last section, we describe some of the current limitations and provide some recommendations for future directions.

Limitations and recommendations

NM-MRI is a promising diagnostic tool and could have the potential to become a component of a precision medicine approach to neurodegenerative and psychiatric diseases. NM-MRI could provide a

stratification tool for predicting treatment success of pharmacological intervention studies targeting the dopaminergic and noradrenergic systems. To date, however, the studies using NM-MRI have only shown group differences, and it is not readily available to evaluate disease status in individuals. Currently, the sensitivity and specificity of NM-MRI measurements are not sufficient for clinical differential diagnosis, and before this technique is incorporated into clinical practice, there are some limitations that need to be addressed.

One of the main limitations of NM-MRI is that it is lacking a standardized protocol for the acquisition and processing of data, a critical step in facilitating large-scale multisite studies and translation into the clinic. The results from studies using NM-MRI are heterogeneous, with inconsistencies between studies, particularly regarding the relationship between changes in NM-MRI signal and disease progression. These differences could be explained by relatively small sample sizes, heterogenous patient sample (e.g. patients at different stages) and differences in image acquisition and processing. NM-MRI is critically dependent on the acquisition sequence and scan parameters. Multiple acquisition protocols, including 2D TSE, and 2D GRE and 3D GRE sequences, have been used, but to date no study has systematically compared the acquisition approaches, and future studies should evaluate the optimal combination of imaging parameters (i.e. power and frequency offset of the MT-pulse, TR, TE, flip angle, size and placement of the field-of-view, in-plane resolution, slice thickness and minimum number of signal averages). Moreover, it is essential to reach expert consensus on technical guidelines for the image acquisition that will allow multicentre data collection and lead to a better validation of NM-MRI as an effective biomarker. Assessments for reproducibility, repeatability, sensitivity, specificity and inter-vendor comparisons still need to be rigorously pursued before clinical adoption.

An important aspect that deserves further investigation is the age-related patterns in NM-MRI signal intensity across the lifespan. Initial studies have suggested an inverted U-shaped cross-sectional relationship with age,[62] replicating the U-shaped cross-sectional development of NM deposits observed in post-mortem tissue.[11] The inverted U-shape has been suggested to reflect increasing NM content due to continuous dopamine and noradrenaline productions during adulthood prior to the advent of age-related neurodegeneration and onset of disease. Future studies should investigate whether higher signal intensities in older adults represent more intact neurons in the SN and LC, and whether other mediating factors for interpreting NM-MRI signal must be considered in different age groups or clinical populations. To date, the sample size of most of the NM-MRI studies are too small to investigate cross-sectional age effects, and studies with larger cohorts[62] are necessary to investigate such relationships.

Understanding the contrast mechanisms associated with NM-MRI should facilitate the clinical interpretation of the measures derived from these images. In neurodegenerative conditions, it has been generally assumed that the decreased contrast in NM-MRI reflects the loss of pigmented dopaminergic neurons in the SNc-VTA and noradrenergic neurons in the LC. However, the mechanism by which the presence of NM might give rise to signal hyperintensities on MRI, and the nature of the relationship between a loss of hyperintensity and cellular integrity of SNc-VTA and LC tissues are still unclear. Moreover, neurodegenerative diseases are also characterized by concurrent pathological processes such as an overall increase of iron content throughout the SN,[155-158] protein aggregation (i.e. Lewy bodies, tau) and neuroinflammation that may confound the observed signal. NM-MRI, like other MRI contrast mechanisms, is determined by processes occurring on molecular and atomic scales and, as a result, it is not specific to any single cellular mechanism. The contrast within a voxel represents a combination of cell types, cellular compartments or even different tissues, and thus, interpretation of NM-MRI results should benefit from supporting data from *in vivo*, post-mortem, *in vitro* and clinical studies[159] requiring the multidisciplinary collaboration of experts in neurodegenerative diseases, imaging, neuropathology and cognition. For example, combining post-mortem multimodal MRI and histological labelling[160] could provide new insights into the underlying biological processes driving *in vivo* NM-MRI results. Recent studies combining quantitative histology and quantitative MRI on post-mortem human brain tissue[159,161,162] showed dominant contributions from the effective transverse relaxation rate ($R2^*$) in the NM of dopaminergic neurons and suggested that the $R2^*$ contribution from dopaminergic neurons reflects the product of cell density and cellular iron concentration. These multidisciplinary efforts can provide a deeper understanding into how NM-MRI contrast relates to biological processes and the pathophysiology of different neurodegenerative diseases. Moreover, integrating *in vivo* imaging with other multiparametric assessments such as fluid biomarkers (e.g. alpha-synuclein seed aggregation assay[163]) can provide further validation and could likely replace traditional and more simplistic approaches to decision-support systems that are currently used in clinical practice.

NM-MRI has the potential to provide insights into the mechanisms underlying catecholamine dysfunction, but currently fails to completely characterize specific biological and pathological changes such as NM content, neuronal loss, protein aggregation and neuroinflammation, limiting its scalability and use in determining the effect of disease-modifying therapies. The last decade has seen new advances in other quantitative MRI techniques, including quantitative magnetization transfer (qMT), quantitative susceptibility mapping (QSM) and multi-compartmental diffusion MRI that may allow detection and quantification of different pathological changes *in vivo*. Future studies should integrate multiple advanced neuroimaging modalities sensitive to different metrics to disassociate the contributions from different cellular compartments (e.g. myelin, intra- and extra-cellular free water) and to increase our ability to interrogate specific mechanisms of neuronal and glial dysfunction.[114]

Future studies should also combine MRI with other imaging modalities such as PET to investigate the relationship between NM-MRI signal and dopamine function along the nigrostriatal network. A couple of studies have investigated the relationship between neuromelanin-sensitive MRI findings and striatal dopamine terminal loss as measured by I-FP-CIT SPECT[123] and have shown a positive correlation with the corresponding striatal I-FP-CIT binding.[65,81,123] A recent study has assessed NM-MRI signal in the SN and dopamine-release in the dorsal striatum in healthy adults (as measured with ^{11}C-raclopride) and inferred a relationship between greater D_2-like receptor displacement and NM-MRI contrast.[15] Additionally, Depierreaux and colleagues[164] linked NM-contrast to increased putaminal dopamine synthesis capacity. A more recent study found correlations between CR values and the standardized uptake value ratio (SUVR) of the posterior putamen using ^{18}F-FP-CIT PET in early-stage Parkinson's disease.[165] These findings suggest that loss of SN signal in NM-MRI is associated with loss of striatal dopamine function and that it can potentially be used as a biomarker of nigrostriatal dysfunction.

One of the main goals of future research is to set up carefully designed longitudinal and multi-site studies in large cohorts of

healthy subjects and patients appropriately phenotyped to assess how the NM-MRI signal is related to brain changes resulting from neurodegeneration or catecholamine dysfunction. Previous studies have revealed moderate to high reproducibility of NM-MRI measures.[58,61,80] Recently, Wengler *et al.*[55,60] proposed a detailed guideline for the image acquisition and analysis and provided recommendations for performing NM-MRI experiments with high quality and reproducibility, providing a foundation for the optimization and standardization of NM-MRI and facilitating large-scale multi-site studies and translation into the clinic. Moreover, harmonization methods that effectively remove non-biological variability, while maintaining biologically relevant variability, should be used when combining NM-MRI data across sites and scanners.[109] Lastly, in an era of artificial intelligence and deep learning techniques, advancements in this field could be exploited for NM-MRI optimization.[84,86,166,167]

In conclusion, NM-MRI is a promising non-invasive and cost-effective tool to investigate human dopaminergic and noradrenergic function *in vivo*, with a wide range of potential clinical applications in neurodegenerative and psychiatric disorders. It has the potential to become a clinically useful biomarker if further evaluated for performance (accuracy, sensitivity, specificity), reproducibility, biological and clinical interpretation. The technical validation should establish if NM-MRI can be obtained reliably at different sites using different scanners, and efforts should be made to harmonize data acquisition and processing. The biological validation should provide evidence that the NM-MRI measures are associated with dopaminergic and noradrenergic function, and the clinical validation should determine the relationship between the imaging measures and the clinical status and progression of patients with neurodegenerative and psychiatric disorders.

Funding

This study was supported by the National Institute of Neurological Disorders and Stroke (1K24AG064114).

Competing interests

The authors report no competing interests.

References

1. Poulin JF, Caronia G, Hofer C, *et al*. Mapping projections of molecularly defined dopamine neuron subtypes using intersectional genetic approaches. *Nat Neurosci*. 2018;21:1260-1271.
2. Calabresi P, Picconi B, Tozzi A, Di Filippo M. Dopamine-mediated regulation of corticostriatal synaptic plasticity. *Trends Neurosci*. 2007;30:211-219.
3. Aston-Jones G, Cohen JD. An integrative theory of locus Coeruleus-norepinephrine function: Adaptive gain and optimal performance. *Annu Rev Neurosci*. 2005;28:403-450.
4. Robbins TW. Cortical noradrenaline, attention and arousal. *Psychol Med*. 1984;14:13-21.
5. Benarroch EE. The locus ceruleus norepinephrine system: Functional organization and potential clinical significance. *Neurology*. 2009;73:1699-1704.
6. Sara SJ. The locus coeruleus and noradrenergic modulation of cognition. *Nat Rev Neurosci*. 2009;10:211-223.
7. Sterpenich V, D'Argembeau A, Desseilles M, *et al*. The locus ceruleus is involved in the successful retrieval of emotional memories in humans. *J Neurosci*. 2006;26:7416-7423.
8. Espay AJ, Lewitt PA, Kaufmann H. Norepinephrine deficiency in Parkinson's disease: The case for noradrenergic enhancement. *Mov Disord*. 2014;29:1710-1719.
9. Sasaki M, Shibata E, Tohyama K, *et al*. Neuromelanin magnetic resonance imaging of locus ceruleus and substantia nigra in Parkinson's disease. *Neuroreport*. 2006;17:1215-1218.
10. Zucca FA, Segura-Aguilar J, Ferrari E, *et al*. Interactions of iron, dopamine and neuromelanin pathways in brain aging and Parkinson's disease. *Prog Neurobiol*. 2017;155:96-119.
11. Zecca L, Youdim MBH, Riederer P, Connor JR, Crichton RR. Iron, brain ageing and neurodegenerative disorders. *Nat Rev Neurosci*. 2004;5:863-873.
12. Sulzer D, Cassidy C, Horga G, *et al*. Neuromelanin detection by magnetic resonance imaging (MRI) and its promise as a biomarker for Parkinson's disease. *NPJ Parkinsons Dis*. 2018;4:11.
13. Kitao S, Matsusue E, Fujii S, *et al*. Correlation between pathology and neuromelanin MR imaging in Parkinson's disease and dementia with Lewy bodies. *Neuroradiology*. 2013;55:947-953.
14. Keren NI, Taheri S, Vazey EM, *et al*. Histologic validation of locus coeruleus MRI contrast in post-mortem tissue. *Neuroimage*. 2015;113:235-245.
15. Cassidy CM, Zucca FA, Girgis RR, *et al*. Neuromelanin-sensitive MRI as a noninvasive proxy measure of dopamine function in the human brain. *Proc Natl Acad Sci USA*. 2019;116:5108-5117.
16. Horga G, Wengler K, Cassidy CM. Neuromelanin-Sensitive magnetic resonance imaging as a proxy marker for catecholamine function in psychiatry. *JAMA Psychiatry*. 2021;78:788.
17. Reneman L, van der Pluijm M, Schrantee A, van de Giessen E. Imaging of the dopamine system with focus on pharmacological MRI and neuromelanin imaging. *Eur J Radiol*. 2021;140:109752.
18. Arribarat G, De Barros A, Péran P. Modern brainstem MRI techniques for the diagnosis of Parkinson's disease and parkinsonisms. *Front Neurol*. 2020;11:791.
19. Arribarat G, Péran P. Quantitative MRI markers in Parkinson's disease and parkinsonian syndromes. *Curr Opin Neurol*. 2020;33:222-229.
20. Betts MJ, Kirilina E, Otaduy MCG, *et al*. Locus coeruleus imaging as a biomarker for noradrenergic dysfunction in neurodegenerative diseases. *Brain*. 2019; 142:2558-2571.
21. Zecca L, Zucca F, Albertini A, Rizzio E, Fariello RG. A proposed dual role of neuromelanin in the pathogenesis of Parkinson' s disease. *Neurology*. 2006;67(7 Suppl 2):S8-11.
22. Sulzer D, Bogulavsky J, Larsen KE, *et al*. Neuromelanin biosynthesis is driven by excess cytosolic catecholamines not accumulated by synaptic vesicles. *Proc Natl Acad Sci U S A*. 2000;97:11869-11874.
23. Zecca L, Bellei C, Costi P, *et al*. New melanic pigments in the human brain that accumulate in aging and block environmental toxic metals. *Proc Natl Acad Sci U S A*. 2008;105:17567-17572.
24. Zhang W, Phillips K, Wielgus AR, *et al*. Neuromelanin activates microglia and induces degeneration of dopaminergic neurons: Implications for progression of Parkinson's disease. *Neurotox Res*. 2011;19:63-72.
25. Zecca L, Stroppolo A, Gatti A, *et al*. The role of iron and copper molecules in the neuronal vulnerability of locus coeruleus and substantia nigra during aging. *Proc Natl Acad Sci U S A*. 2004;101:9843-9848.
26. Zecca L, Swartz HM. Total and paramagnetic metals in human substantia nigra and its neuromelanin. *J Neural Transm Park Dis Dement Sect*. 1993;5:203-213.

27. Kaiya H. Neuromelanin, neuroleptics and schizophrenia. *Neuropsychobiology*. 1980;6:241-248.
28. Watanabe Y, Tanaka H, Tsukabe A, *et al*. Neuromelanin magnetic resonance imaging reveals increased dopaminergic neuron activity in the substantia Nigra of patients with schizophrenia. *PLoS One*. 2014;9:e104619.
29. Cassidy CM, Carpenter KM, Konova AB, *et al*. Evidence for dopamine abnormalities in the substantia Nigra in cocaine addiction revealed by neuromelanin-sensitive MRI. *Am J Psychiat*. 2020;177:1038-1047.
30. Watanabe T, Wang X, Tan Z, Frahm J. Magnetic resonance imaging of brain cell water. *Sci Rep*. 2019;9:5084.
31. Watanabe T, Tan Z, Wang X, Martinez-Hernandez A, Frahm J. Magnetic resonance imaging of noradrenergic neurons. *Brain Struct Funct*. 2019;224:1609-1625.
32. Watanabe T, Frahm J. Gadobutrol enhances T 1 -weighted MRI of nerve cells. *Toxicol Lett*. 2019;308:17-23.
33. Priovoulos N, van Boxel SCJ, Jacobs HIL, *et al*. Unraveling the contributions to the neuromelanin-MRI contrast. *Brain Struct Funct*. 2020;225:2757-2774.
34. He N, Chen Y, LeWitt PA, Yan F, Haacke EM. Response to "neuromelanin? MRI of noradrenergic and dopaminergic neurons". *J Magn Reson Imaging*. 2023;58:326-327.
35. Watanabe T. Neuromelanin? MRI of noradrenergic and dopaminergic neurons. *J Magn Reson Imaging*. 2023;58:328-329.
36. Enochs W, Petherick P, Bogdanova A, Mohr U, Weissleder R. Paramagnetic metal scavenging by melanin: MR imaging. *Radiology*. 1997;204:417-423.
37. Enochs WS, Hyslop WB, Bennett HF, Brown RD, Koenig SH, Swartz HM. Sources of the increased longitudinal relaxation rates observed in melanotic melanoma. An in vitro study of synthetic melanins. *Invest Radiol*. 1989;24:794-804.
38. Tosk JM, Holshouser BA, Aloia RC, *et al*. Effects of the interaction between ferric iron and L-dopa melanin on T1 and T2 relaxation times determined by magnetic resonance imaging. *Magn Reson Med*. 1992;26:40-45.
39. Trujillo P, Summers PE, Ferrari E, *et al*. Contrast mechanisms associated with neuromelanin-MRI. *Magn Reson Med*. 2017;78:1790-1800.
40. Nakane T, Nihashi T, Kawai H, Naganawa S. Visualization of neuromelanin in the substantia nigra and locus ceruleus at 1.5T using a 3D-gradient echo sequence with magnetization transfer contrast. *Magn Reson Med Sci*. 2008;7:205-210.
41. Hashido T, Saito S. Quantitative T1, T2, and T2* mapping and semi-quantitative neuromelanin-sensitive magnetic resonance imaging of the human midbrain. *PLoS One*. 2016;11:e0165160.
42. Schwarz ST, Bajaj N, Morgan PS, Reid S, Gowland P, Auer DP. Magnetisation transfer contrast to enhance detection of neuromelanin loss at 3T in Parkinson's disease. *Proc Intl Soc Mag Reson Med* 2013;21:2848.
43. Langley J, Huddleston DE, Chen X, Sedlacik J, Zachariah N, HuX. A multicontrast approach for comprehensive imaging of substantia nigra. *Neuroimage*. 2015;112:7-13.
44. Dixon WT, Engels H, Castillo M, Sardashti M. Incidental magnetization transfer contrast in standard multislice imaging. *Magn Reson Imaging*. 1990;8:417-422.
45. Priovoulos N, Jacobs HIL, Ivanov D, Uludağ K, Verhey FRJ, Poser BA. High-resolution in vivo imaging of human locus coeruleus by magnetization transfer MRI at 3T and 7T. *Neuroimage*. 2018;168:427-436.
46. Tona KD, van Osch MJP, Nieuwenhuis S, Keuken MC. Quantifying the contrast of the human locus coeruleus in vivo at 7 tesla MRI. *PLoS One*. 2019;14:e0209842.
47. Henkelman RM, Huang X, Xiang QS, Stanisz GJ, Swanson SD, Bronskill MJ. Quantitative interpretation of magnetization transfer. *Magn Reson Med*. 1993;29:759-766.
48. Thomas SD, Al-Kwifi O, Emery DJ, Wilman AH. Application of magnetization transfer at 3.0 T in three-dimensional time-of-flight magnetic resonance angiography of the intracranial arteries. *J Magn Reson Imaging*. 2002;15:479-483.
49. Trujillo P, Summers PE, Smith AK, *et al*. Pool size ratio of the substantia nigra in Parkinson's disease derived from two different quantitative magnetization transfer approaches. *Neuroradiology*. 2017;59:1251-1263.
50. Trujillo P, Smith AK, Summers PE, *et al*. High-resolution quantitative imaging of the substantia nigra. *Ann Int Conf Proc IEEE Eng Med Biol Soc*. 2015;2015:5428-5431.
51. Trujillo P, Petersen KJ, Cronin MJ, *et al*. Quantitative magnetization transfer imaging of the human locus coeruleus. *Neuroimage*. 2019;200:191-198.
52. Ogisu K, Kudo K, Sasaki M, *et al*. 3D neuromelanin-sensitive magnetic resonance imaging with semi-automated volume measurement of the substantia nigra pars compacta for diagnosis of Parkinson's disease. *Neuroradiology*. 2013;55:719-724.
53. Chen X, Huddleston DE, Langley J, *et al*. Simultaneous imaging of locus coeruleus and substantia nigra with a quantitative neuromelanin MRI approach. *Magn Reson Imaging*. 2014;32:1301-1306.
54. Schwarz ST, Rittman T, Gontu V, Morgan PS, Bajaj N, Auer DDP. T1-weighted MRI shows stage-dependent substantia nigra signal loss in Parkinson's disease. *Mov Disord*. 2011;26:1633-1638.
55. Wengler K, He X, Abi-Dargham A, Horga G. Reproducibility assessment of neuromelanin-sensitive magnetic resonance imaging protocols for region-of-interest and voxelwise analyses. *Neuroimage*. 2020;208:116457.
56. Liu Y, Li J, He N, *et al*. Optimizing neuromelanin contrast in the substantia nigra and locus coeruleus using a magnetization transfer contrast prepared 3D gradient recalled echo sequence. *Neuroimage*. 2020;218:116935.
57. Liu KY, Marijatta F, Hämmerer D, Acosta-Cabronero J, Düzel E, Howard RJ. Magnetic resonance imaging of the human locus coeruleus: A systematic review. *Neurosci Biobehav Rev*. 2017;83:325-355.
58. Betts MJ, Cardenas-Blanco A, Kanowski M, Jessen F, Düzel E. In vivo MRI assessment of the human locus coeruleus along its rostrocaudal extent in young and older adults. *Neuroimage*. 2017;163:150-159.
59. Wengler K, Ashinoff BK, Pueraro E, Cassidy CM, Horga G, Rutherford BR. Association between neuromelanin-sensitive MRI signal and psychomotor slowing in late-life depression. *Neuropsychopharmacology*. 2021;46:1233-1239.
60. Salzman G, Kim J, Horga G, Wengler K. Standardized data acquisition for neuromelanin-sensitive magnetic resonance imaging of the substantia nigra. *J Vis Exp*. 2021;175:10.3791/62493.
61. Tona KD, Keuken MC, de Rover M, *et al*. In vivo visualization of the locus coeruleus in humans: Quantifying the test–retest reliability. *Brain Struct Funct*. 2017;222:4203-4217.
62. Liu KY, Acosta-Cabronero J, Cardenas-Blanco A, *et al*. In vivo visualization of age-related differences in the locus coeruleus. *Neurobiol Aging*. 2019;74:101-111.
63. Pyatigorskaya N, Magnin B, Mongin M, *et al*. Comparative study of MRI biomarkers in the substantia Nigra to discriminate idiopathic Parkinson disease. *Am J Neuroradiol*. 2018;39:1460-1467.
64. Liu XL, Yang LQ, Liu FT, *et al*. Short-echo-time magnitude image derived from quantitative susceptibility mapping could resemble neuromelanin-sensitive MRI image in substantia nigra. *BMC Neurol*. 2020;20:262.

65. Kuya K, Shinohara Y, Miyoshi F, Fujii S, Tanabe Y, Ogawa T. Correlation between neuromelanin-sensitive MR imaging and (123)I-FP-CIT SPECT in patients with parkinsonism. *Neuroradiology*. 2016;58:351-356.
66. Kashihara K, Shinya T, Higaki F. Reduction of neuromelanin-positive nigral volume in patients with MSA, PSP and CBD. *Intern Med*. 2011;50:1683-1687.
67. Kashihara K, Shinya T, Higaki F. Neuromelanin magnetic resonance imaging of nigral volume loss in patients with Parkinson's disease. *J Clin Neurosci*. 2011;18:1093-1096.
68. Gaurav R, Yahia-Cherif L, Pyatigorskaya N, *et al*. Longitudinal changes in neuromelanin MRI signal in Parkinson's disease: A progression marker. *Mov Disord*. 2021;36:1592-1602.
69. Kuya K, Ogawa T, Shinohara Y, *et al*. Evaluation of Parkinson's disease by neuromelanin-sensitive magnetic resonance imaging and 123 I-FP-CIT SPECT. *Acta radiol*. 2018;59:593-598.
70. Miyoshi F, Ogawa T, Kitao SI, *et al*. Evaluation of Parkinson disease and Alzheimer disease with the use of neuromelanin MR imaging and 123I-metaiodobenzylguanidine scintigraphy. *AJNR Am J Neuroradiol*. 2013;34:2113-2118.
71. Ohtsuka C, Sasaki M, Konno K, *et al*. Differentiation of early-stage parkinsonisms using neuromelanin-sensitive magnetic resonance imaging. *Parkinsonism Relat Disord*. 2014;20:755-760.
72. Xiang Y, Gong T, Wu J, *et al*. Subtypes evaluation of motor dysfunction in Parkinson's disease using neuromelanin-sensitive magnetic resonance imaging. *Neurosci Lett*. 2017;638:145-150.
73. Prasad S, Stezin A, Lenka A, *et al*. Three-dimensional neuromelanin-sensitive magnetic resonance imaging of the substantia nigra in Parkinson's disease. *Eur J Neurol*. 2018;25:680-686.
74. Matsuura K, Maeda M, Yata K, *et al*. Neuromelanin magnetic resonance imaging in Parkinson's disease and multiple system atrophy. *Eur Neurol*. 2013;70:70-77.
75. Ohtsuka C, Sasaki M, Konno K, *et al*. Changes in substantia nigra and locus coeruleus in patients with early-stage Parkinson's disease using neuromelanin-sensitive MR imaging. *Neurosci Lett*. 2013;541:93-98.
76. Castellanos G, Fernández-Seara MA, Lorenzo-Betancor O, *et al*. Automated neuromelanin imaging as a diagnostic biomarker for Parkinson's disease. *Mov Disord*. 2015;30:945-952.
77. Fabbri M, Reimão S, Carvalho M, *et al*. Substantia Nigra neuromelanin as an imaging biomarker of disease progression in Parkinson's disease. *J Parkinsons Dis*. 2017;7:491-501.
78. Takahashi H, Watanabe Y, Tanaka H, *et al*. Comprehensive MRI quantification of the substantia nigra pars compacta in Parkinson's disease. *Eur J Radiol*. 2018;109:48-56.
79. Zupan G, Šuput D, Pirtošek Z, Vovk A. Semi-Automatic signature-based segmentation method for quantification of neuromelanin in substantia Nigra. *Brain Sci*. 2019;9:335.
80. Langley J, Huddleston DE, Liu CJ, Hu X. Reproducibility of locus coeruleus and substantia nigra imaging with neuromelanin sensitive MRI. *MAGMA*. 2017;30:121-125.
81. Isaias IU, Trujillo P, Summers P, *et al*. Neuromelanin imaging and dopaminergic loss in Parkinson's disease. *Front Aging Neurosci*. 2016;8:196.
82. Safai A, Prasad S, Chougule T, Saini J, Pal PK, Ingalhalikar M. Microstructural abnormalities of substantia nigra in Parkinson's disease: A neuromelanin sensitive MRI atlas based study. *Hum Brain Mapp*. 2020;41:1323-1333.
83. Ariz M, Abad RC, Castellanos G, *et al*. Dynamic atlas-based segmentation and quantification of neuromelanin-rich brainstem structures in Parkinson disease. *IEEE Trans Med Imaging*. 2019;38:813-823.
84. Krupička R, Mareček S, Malá C, *et al*. Automatic substantia nigra segmentation in neuromelanin-sensitive MRI by deep neural network in patients with prodromal and manifest synucleinopathy. *Physiol Res*. 2019;68(Suppl 4):S453-S458.
85. Le Berre A, Kamagata K, Otsuka Y, *et al*. Convolutional neural network-based segmentation can help in assessing the substantia nigra in neuromelanin MRI. *Neuroradiology*. 2019;61:1387-1395.
86. Gaurav R, Pyatigorskaya N, Biondetti E, *et al*. Deep learning-based neuromelanin MRI changes of isolated REM sleep behavior disorder. *Mov Disord*. 2022;37:1064-1069.
87. Sasaki M, Shibata E, Ohtsuka K, *et al*. Visual discrimination among patients with depression and schizophrenia and healthy individuals using semiquantitative color-coded fast spin-echo T1-weighted magnetic resonance imaging. *Neuroradiology*. 2010;52:83-89.
88. Ehrminger M, Latimier A, Pyatigorskaya N, *et al*. The coeruleus/subcoeruleus complex in idiopathic rapid eye movement sleep behaviour disorder. *Brain*. 2016;139:1180-1188.
89. García-Lorenzo D, Longo-Dos Santos C, Ewenczyk C, *et al*. The coeruleus/subcoeruleus complex in rapid eye movement sleep behaviour disorders in Parkinson's disease. *Brain*. 2013;136:2120-2129.
90. Keren N, Lozar C, Harris K, Morgan P, Eckert M. In vivo mapping of the human locus coeruleus. *Neuroimage*. 2009;47:1261-1267.
91. Sommerauer M, Fedorova TD, Hansen AK, *et al*. Evaluation of the noradrenergic system in Parkinson's disease: An 11C-MeNER PET and neuromelanin MRI study. *Brain*. 2018;141:496-504.
92. Ye R, Rua C, O'Callaghan C, *et al*. An in vivo probabilistic atlas of the human locus coeruleus at ultra-high field. *Neuroimage*. 2021;225:117487.
93. Reimão S, Pita Lobo P, Neutel D, *et al*. Substantia nigra neuromelanin magnetic resonance imaging in de novo Parkinson's disease patients. *Eur J Neurol*. 2015;22:540-546.
94. Reimão S, Pita Lobo P, Neutel D, *et al*. Substantia nigra neuromelanin-MR imaging differentiates essential tremor from Parkinson's disease. *Mov Disord*. 2015;30:953-959.
95. Hatano T, Okuzumi A, Kamagata K, *et al*. Neuromelanin MRI is useful for monitoring motor complications in Parkinson's and PARK2 disease. *J Neural Transm*. 2017;124:407-415.
96. Takahashi H, Watanabe Y, Tanaka H, *et al*. Quantifying changes in nigrosomes using quantitative susceptibility mapping and neuromelanin imaging for the diagnosis of early-stage Parkinson's disease. *Br J Radiol*. 2018;91:20180037.
97. Matsuura K, Maeda M, Tabei KI, *et al*. A longitudinal study of neuromelanin-sensitive magnetic resonance imaging in Parkinson's disease. *Neurosci Lett*. 2016;633:112-117.
98. Taniguchi D, Hatano T, Kamagata K, *et al*. Neuromelanin imaging and midbrain volumetry in progressive supranuclear palsy and Parkinson's disease. *Mov Disord*. 2018;33:1488-1492.
99. Reimão S, Pita Lobo P, Neutel D, *et al*. Quantitative analysis versus visual assessment of neuromelanin MR imaging for the diagnosis of Parkinson's disease. *J Parkinsons Dis*. 2015;5:561-567.
100. Reimão S, Ferreira S, Nunes RG, *et al*. Magnetic resonance correlation of iron content with neuromelanin in the substantia nigra of early-stage Parkinson's disease. *Eur J Neurol*. 2016;23:368-374.
101. Wang J, Huang Z, Li Y, *et al*. Neuromelanin-sensitive MRI of the substantia nigra: An imaging biomarker to differentiate essential tremor from tremor-dominant Parkinson's disease. *Parkinsonism Relat Disord*. 2019;58:3-8.

102. Wang J, Li Y, Huang Z, *et al*. Neuromelanin-sensitive magnetic resonance imaging features of the substantia nigra and locus coeruleus in de novo Parkinson's disease and its phenotypes. *Eur J Neurol*. 2018;25:949-e73.
103. Moon WJ, Park JY, Yun WS, *et al*. A comparison of substantia nigra T1 hyperintensity in Parkinson's disease dementia, Alzheimer's disease and age-matched controls: Volumetric analysis of neuromelanin imaging. *Korean J Radiol*. 2016;17: 633-640.
104. Pyatigorskaya N, Gaurav R, Arnaldi D, *et al*. Magnetic resonance imaging biomarkers to assess substantia Nigra damage in idiopathic rapid eye movement sleep behavior disorder. *Sleep*. 2017;40:1-8.
105. Schwarz ST, Xing Y, Tomar P, Bajaj N, Auer DP. In vivo assessment of brainstem depigmentation in Parkinson disease: Potential as a severity marker for multicenter studies. *Radiology*. 2017;283:789-798.
106. Clewett DV, Lee TH, Greening S, Ponzio A, Margalit E, Mather M. Neuromelanin marks the spot: Identifying a locus coeruleus biomarker of cognitive reserve in healthy aging. *Neurobiol Aging*. 2016;37:117-126.
107. Tanaka M, Aihara YY, Ikeda S, Aihara YY. [Neuromelanin-related contrast in the substantia nigra semiquantitatively evaluated by magnetic resonance imaging at 3T: Comparison between normal aging and Parkinson disease]. *Rinsho Shinkeigaku*. 2011;51:14-20.
108. Huddleston DE, Langley J, Sedlacik J, Boelmans K, Factor SA, Hu XP. In vivo detection of lateral–ventral tier nigral degeneration in Parkinson's disease. *Hum Brain Mapp*. 2017;38:2627-2634.
109. Wengler K, Cassidy C, van der Pluijm M, *et al*. Cross-Scanner harmonization of neuromelanin-sensitive MRI for multisite studies. *J Magn Reson Imaging*. 2021;54:1189-1199.
110. Cho SJ, Bae YJ, Kim JM, *et al*. Diagnostic performance of neuromelanin-sensitive magnetic resonance imaging for patients with Parkinson's disease and factor analysis for its heterogeneity: A systematic review and meta-analysis. *Eur Radiol*. 2021;31:1268-1280.
111. Wang X, Zhang Y, Zhu C, *et al*. The diagnostic value of SNpc using NM-MRI in Parkinson's disease: Meta-analysis. *Neurol Sci*. 2019;40:2479-2489.
112. Sung YH, Noh Y, Kim EY. Early-stage Parkinson's disease: Abnormal nigrosome 1 and 2 revealed by a voxelwise analysis of neuromelanin-sensitive MRI. *Hum Brain Mapp*. 2021;42: 2823-2832.
113. Ben Bashat D, Thaler A, Lerman Shacham H, *et al*. Neuromelanin and T2*-MRI for the assessment of genetically at-risk, prodromal, and symptomatic Parkinson's disease. *NPJ Parkinsons Dis*. 2022;8:139.
114. He N, Ghassaban K, Huang P, *et al*. Imaging iron and neuromelanin simultaneously using a single 3D gradient echo magnetization transfer sequence: Combining neuromelanin, iron and the nigrosome-1 sign as complementary imaging biomarkers in early stage Parkinson's disease. *Neuroimage*. 2021;230: 117810.
115. Bae YJ, Kim JM, Sohn CH, *et al*. Imaging the substantia Nigra in Parkinson disease and other parkinsonian syndromes. *Radiology*. 2021;300:260-278.
116. Biondetti E, Gaurav R, Yahia-Cherif L, *et al*. Spatiotemporal changes in substantia nigra neuromelanin content in Parkinson's disease. *Brain*. 2020;143:2757-2770.
117. Xing Y, Sapuan AH, Martín-Bastida A, *et al*. Neuromelanin-MRI to quantify and track nigral depigmentation in Parkinson's disease: A multicenter longitudinal study using template-based standardized analysis. *Mov Disord*. 2022;37:1028-1039.
118. Furukawa K, Shima A, Kambe D, *et al*. Motor progression and nigrostriatal neurodegeneration in Parkinson disease. *Ann Neurol*. 2022;92:110-121.
119. Wang S, Wu T, Cai Y, Yu Y, Chen X, Wang L. Neuromelanin magnetic resonance imaging of substantia nigra and locus coeruleus in Parkinson's disease with freezing of gait. *Front Aging Neurosci*. 2023;15:44.
120. Su D, Gan Y, Zhang Z, *et al*. Multimodal imaging of substantia Nigra in Parkinson's disease with levodopa-induced dyskinesia. *Mov Disord*. 2023;38:616-625.
121. Prasuhn J, Prasuhn M, Fellbrich A, *et al*. Association of locus Coeruleus and substantia Nigra pathology with cognitive and motor functions in patients with Parkinson disease. *Neurology*. 2021;97:e1007-e1016.
122. Madelung CF, Meder D, Fuglsang SA, *et al*. Locus Coeruleus shows a spatial pattern of structural disintegration in Parkinson's disease. *Mov Disord*. 2022;37:479-489.
123. Ryman SG, Poston KL. MRI Biomarkers of motor and non-motor symptoms in Parkinson's disease. *Parkinsonism Relat Disord*. 2020;73:85-93.
124. Matsuura K, Ii Y, Maeda M, *et al*. Neuromelanin-sensitive magnetic resonance imaging in disease differentiation for parkinsonism or neurodegenerative disease affecting the basal ganglia. *Parkinsonism Relat Disord*. 2021;87:75-81.
125. Pyatigorskaya N, Yahia-Cherif L, Gaurav R, *et al*. Multimodal magnetic resonance imaging quantification of brain changes in progressive supranuclear palsy. *Mov Disord*. 2020;35:161-170.
126. Iranzo A, Fernández-Arcos A, Tolosa E, *et al*. Neurodegenerative disorder risk in idiopathic REM sleep behavior disorder: Study in 174 patients. *PLoS One*. 2014;9:e89741.
127. Biondetti E, Santin MD, Valabrègue R, *et al*. The spatiotemporal changes in dopamine, neuromelanin and iron characterizing Parkinson's disease. *Brain*. 2021;144:3114-3125.
128. Britton TC, Chaudhuri KR. REM Sleep behavior disorder and the risk of developing Parkinson disease or dementia. *Neurology*. 2009;72:1294-1295.
129. Plazzi G, Corsini R, Provini F, *et al*. REM Sleep behavior disorders in multiple system atrophy. *Neurology*. 1997;48:1094-1097.
130. St Louis EK, Boeve AR, Boeve BF. REM Sleep behavior disorder in Parkinson's disease and other synucleinopathies. *Mov Disord*. 2017;32:645-658.
131. Knudsen K, Fedorova TD, Hansen AK, *et al*. In-vivo staging of pathology in REM sleep behaviour disorder: A multimodality imaging case-control study. *Lancet Neurol*. 2018;17:618-628.
132. Tomlinson BE, Irving D, Blessed G. Cell loss in the locus coeruleus in senile dementia of Alzheimer type. *J Neurol Sci*. 1981;49: 419-428.
133. Bondareff W, Mountjoy CQ, Roth M. Selective loss of neurones of origin of adrenergic projection to cerebral cortex (nucleus locus coeruleus) in senile dementia. *Lancet*. 1981;1:783-784.
134. German DC, Manaye KF, White CL, *et al*. Disease-specific patterns of locus coeruleus cell loss. *Ann Neurol*. 1992;32:667-676.
135. Beardmore R, Hou R, Darekar A, Holmes C, Boche D. The locus Coeruleus in aging and Alzheimer's disease: A postmortem and brain imaging review. *J Alzheimers Dis*. 2021;83:5-22.
136. German DC, Walker BS, Manaye K, Smith WK, Woodward DJ, North AJ. The human locus coeruleus: Computer reconstruction of cellular distribution. *J Neurosci*. 1988;8:1776-1788.
137. Marcyniuk B, Mann DMA, Yates PO. Loss of nerve cells from locus coeruleus in Alzheimer's disease is topographically arranged. *Neurosci Lett*. 1986;64:247-252.
138. Theofilas P, Ehrenberg AJ, Dunlop S, *et al*. Locus coeruleus volume and cell population changes during Alzheimer's disease progression: A stereological study in human postmortem

brains with potential implication for early-stage biomarker discovery. *Alzheimers Dement*. 2017;13:236-246.
139. Ehrenberg AJ, Nguy AK, Theofilas P, *et al*. Quantifying the accretion of hyperphosphorylated tau in the locus coeruleus and dorsal raphe nucleus: The pathological building blocks of early Alzheimer's disease. *Neuropathol Appl Neurobiol*. 2017; 43:393-408.
140. Braak H, Ghebremedhin E, Rüb U, Bratzke H, Del Tredici K. Stages in the development of Parkinson's disease-related pathology. *Cell Tissue Res*. 2004;318:121-134.
141. Andrés-Benito P, Fernández-Dueñas V, Carmona M, *et al*. Locus coeruleus at asymptomatic early and middle braak stages of neurofibrillary tangle pathology. *Neuropathol Appl Neurobiol*. 2017;43:373-392.
142. Hou R, Beardmore R, Holmes C, Osmond C, Darekar A. A case-control study of the locus coeruleus degeneration in Alzheimer's disease. *Eur Neuropsychopharmacol*. 2021;43:153-159.
143. Takahashi J, Shibata T, Sasaki M, *et al*. Detection of changes in the locus coeruleus in patients with mild cognitive impairment and Alzheimer's disease: High-resolution fast spin-echo T1-weighted imaging. *Geriatr Gerontol Int*. 2015;15:334-340.
144. Cassidy CM, Therriault J, Pascoal TA, *et al*. Association of locus coeruleus integrity with braak stage and neuropsychiatric symptom severity in Alzheimer's disease. *Neuropsychopharmacology*. 2022;47:1128-1136.
145. Wieland L, Fromm S, Hetzer S, Schlagenhauf F, Kaminski J. Neuromelanin-Sensitive magnetic resonance imaging in schizophrenia: A meta-analysis of case-control studies. *Front Psychiatry*. 2021;12:770282.
146. Ueno F, Iwata Y, Nakajima S, *et al*. Neuromelanin accumulation in patients with schizophrenia: A systematic review and meta-analysis. *Neurosci Biobehav Rev*. 2022;132:1205-1213.
147. Shibata E, Sasaki M, Tohyama K, Otsuka K, Sakai A. Reduced signal of locus ceruleus in depression in quantitative neuromelanin magnetic resonance imaging. *Neuroreport*. 2007;18: 415-418.
148. Shibata E, Sasaki M, Tohyama K, *et al*. Use of neuromelanin-sensitive MRI to distinguish schizophrenic and depressive patients and healthy individuals based on signal alterations in the substantia Nigra and locus ceruleus. *Biol Psychiatry*. 2008; 64:401-406.
149. Carter CS. Further evidence that MRI based measurement of midbrain neuromelanin may serve as a proxy measure of brain dopamine activity in psychiatric disorders. *Neuropsychopharmacology*. 2021;46:1231-1232.
150. Tavares M, Reimão S, Chendo I, Carvalho M, Levy P, Nunes RG. Neuromelanin magnetic resonance imaging of the substantia nigra in first episode psychosis patients consumers of illicit substances. *Schizophr Res*. 2018;197:620-621.
151. Shibata E, Sasaki M, Tohyama K, *et al*. Age-related changes in locus ceruleus on neuromelanin magnetic resonance imaging at 3 tesla. *Magn Reson Med Sci*. 2006;5:197-200.
152. Xing Y, Sapuan A, Dineen RA, Auer DP. Life span pigmentation changes of the substantia nigra detected by neuromelanin-sensitive MRI. *Mov Disord*. 2018;33:1792-1799.
153. Elman JA, Puckett OK, Beck A, *et al*. MRI-assessed locus coeruleus integrity is heritable and associated with multiple cognitive domains, mild cognitive impairment, and daytime dysfunction. *Alzheimer's and Dementia*. 2021;17:1017-1025.
154. Biomarkers Definitions Working Group. Biomarkers and surrogate endpoints: Preferred definitions and conceptual framework. *Clin Pharmacol Ther*. 2001;69:89-95.
155. Dexter DT, Wells FR, Agid F, *et al*. Increased nigral iron content in postmortem parkinsonian brain. *Lancet*. 1987;2:1219-1220.
156. Dexter D, Wells F, Lees A, *et al*. Increased nigral iron content and alterations in other metal ions occurring in brain in Parkinson's disease. *J Neurochem*. 1989;52:1830-1836.
157. Earle K. Studies on Parkinson's disease including x-ray fluorescent spectroscopy of formalin fixed brain tissue. *J Neuropathol Exp Neurol*. 1968;27:1-14.
158. Sofic E, Riederer P, Heinsen H, *et al*. Increased iron (III) and total iron content in post mortem substantia nigra of parkinsonian brain. *J Neural Transm*. 1988;74:199-205.
159. Brammerloh M, Morawski M, Friedrich I, *et al*. Measuring the iron content of dopaminergic neurons in substantia nigra with MRI relaxometry. *Neuroimage*. 2021;239:118255.
160. Forstmann BU, De Hollander G, Van Maanen L, Alkemade A, Keuken MC. Towards a mechanistic understanding of the human subcortex. *Nat Rev Neurosci*. 2016;18:57-65.
161. Lee H, Baek SY, Kim EJ, Huh GY, Lee JH, Cho HJ. MRI T2 and T2* relaxometry to visualize neuromelanin in the dorsal substantia nigra pars compacta. *Neuroimage*. 2020;211: 116625.
162. Lee H, Baek SY, Chun SY, Lee JH, Cho HJ. Specific visualization of neuromelanin-iron complex and ferric iron in the human post-mortem substantia nigra using MR relaxometry at 7T. *Neuroimage*. 2018;172:874-885.
163. Siderowf A, Concha-Marambio L, Lafontant DE, *et al*. Assessment of heterogeneity among participants in the Parkinson's progression markers initiative cohort using α-synuclein seed amplification: A cross-sectional study. *Lancet Neurol*. 2023;22:407-417.
164. Depierreux F, Parmentier E, Mackels L, *et al*. Parkinson's disease multimodal imaging: F-DOPA PET, neuromelanin-sensitive and quantitative iron-sensitive MRI. *NPJ Parkinsons Dis*. 2021;7:57.
165. Park S, Sung YH, Kim WR, Noh Y, Kim EY. Correlation between neuromelanin-sensitive MRI and 18F-FP-CIT PET in early-stage Parkinson's disease: Utility of a voxel-wise analysis by using high-spatial-resolution MRI. *J Clin Neurol*. 2023; 19:156-164.
166. Oshima S, Fushimi Y, Miyake KK, *et al*. Denoising approach with deep learning-based reconstruction for neuromelanin-sensitive MRI: Image quality and diagnostic performance. *Jpn J Radiol*. 2023; 11:1216-1225.
167. Dünnwald M, Ernst P, Düzel E, Tönnies K, Betts MJ, Oeltze-Jafra S. Fully automated deep learning-based localization and segmentation of the locus coeruleus in aging and Parkinson's disease using neuromelanin-sensitive MRI. *Int J Comput Assist Radiol Surg*. 2021;16:2129-2135.